Available online at www.sciencedirect.com
SCIENCE DIRECT®
ELSEVIER
International Journal of Solids and Structures 42 (2005) 5097–5117
INTERNATIONAL JOURNAL OF SOLIDS and STRUCTURES
www.elsevier.com/locate/ijsolstr

On ductile fracture initiation toughness: Effects of void volume fraction, void shape and void distribution

Xiaosheng Gao *, Tianhong Wang, Jinkook Kim

Department of Mechanical Engineering, The University of Akron, 302 Buchtel Mall, Akron, OH 44325, USA

Received 10 August 2004; received in revised form 17 February 2005
Available online 28 March 2005

Abstract

This paper studies the effects of the initial relative void spacing, void pattern, void shape and void volume fraction on ductile fracture toughness using three-dimensional, small scale yielding models, where voids are assumed to pre-exist in the material and are explicitly modeled using refined finite elements. Results of this study can be used to explain the observed fracture toughness anisotropy in industrial alloys. Our analyses suggest that simplified models containing a single row of voids ahead of the crack tip is sufficient when the initial void volume fraction remains small. When the initial void volume fraction becomes large, these simplified models can predict the fracture initiation toughness (J_{Ic}) with adequate accuracy but cannot predict the correct J–R curve because they over-predict the interaction among growing voids on the plane of crack propagation. Consequently, finite element models containing multiple rows of voids should be used when the material has large initial void volume fraction.

Keywords: Ductile fracture; Void growth and coalescence; Fracture toughness; Void shape; Void volume fraction; Relative void spacing; Void pattern; Finite element analysis

1. Introduction

Ductile fracture of many structural materials is a result of void nucleation, growth and coalescence. In practical applications, the J-integral value at the initiation of crack growth, J_{Ic}, is often used as an important parameter to characterize the toughness of ductile materials. Micromechanics analysis of the fracture process makes it possible to link the macroscopic fracture toughness and the microstructure of the material. Two types of the mechanism-based approaches have been proposed in the literature to predict fracture

* Corresponding author. Tel.: +1 330 972 2415; fax: +1 330 972 6027.
E-mail address: xgao@uakron.edu (X. Gao).

0020-7683/$ - see front matter © 2005 Elsevier Ltd. All rights reserved.
doi:10.1016/j.ijsolstr.2005.02.028

toughness. In the first approach, voids are considered implicitly by using continuum damage material models, e.g., the Gurson–Tvergaard model (Gurson, 1977; Tvergaard, 1982). This approach is attractive for simulation of extensive crack growth because detailed modeling of each individual void is avoided (Brocks et al., 1995; Xia et al., 1995; Gao et al., 1998a,b). However, the primary disadvantage of this approach is that a precise constitutive model for characterization of the void-containing material behavior during the ductile fracture process is needed.

In the second approach, voids are considered explicitly and modeled using refined finite elements. A distinct advantage of this approach is the exact implementation of void growth behavior. In order to establish crack advance, a failure criterion for the ligament between a void and the crack tip is required. Rice and Johnson (1969) proposed that coalescence occurs when the size of the ligament between the crack tip and the void becomes equal to the vertical diameter of the void. Brown and Embury (1973) suggested that as soon as the spacing of neighboring voids becomes equal to their length, a slip plane can be drawn between the voids and the localized plastic flow causes ligament failure. Le Roy et al. (1981) proposed that void linkage occurs when the longest axis of the void is of the order of magnitude of the mean planar neighbor spacing. Koplik and Needleman (1988) put forth a method to determine the onset of void coalescence by conducting unit cell analysis. Coalescence (internal necking) occurs when the macroscopic deformation of the unit cell shifts to a uniaxial straining state.

The disadvantage of the explicit approach is due to computational limitations, only a limited number of voids can be included in the crack tip region. The published literatures in this area are mainly two-dimensional. Aravas and McMeeking (1985a,b) examined the interaction between the crack tip and a cylindrical void under the plane strain, small scale yielding (SSY) conditions and estimated the fracture initiation toughness using the coalescence models by Rice and Johnson (1969), Brown and Embury (1973) and Le Roy et al. (1981). Yan and Mai (1998) analyzed the growth of a single cylindrical void ahead of a blunt crack tip in the single-edge-notch bending specimens with different crack lengths. Arun and Narasimhan (1999) investigated the effect of crack tip constraint on void growth under mixed modes I and II loading. In these studies, only a single void is presented in the crack tip region. More recently, Gu (2000) considered a row of six cylindrical voids ahead of the crack tip of the compact tension and center-cracked tension specimens and discussed the effects of specimen geometry, crack length and specimen size on the J–R curve. Tvergaard and Hutchinson (2002) investigated two distinct mechanisms for ductile crack initiation and growth, the void by void growth mechanism and the multiple void interaction mechanism, by considering a row of cylindrical voids ahead of a plane strain, SSY crack tip. They found that transition of the two mechanisms is primary governed by the initial void volume fraction. For materials having smaller initial void volume fraction, interaction occurs only between the crack tip and the nearest void and crack growth follows a void by void mechanism. For materials with larger initial void volume fraction, simultaneous interaction of multiple voids ahead of the crack tip occurs both during initiation and subsequent crack growth.

Published literatures on three-dimensional analysis of ductile fracture process using the explicit approach are relatively limited. Kuna and Sun (1996) investigated the influence of void arrangement on the macroscopic deformation and softening behavior of a unit cell and found that the 3D plane strain model containing a spherical void is stiffer than the 2D plane strain model having a cylindrical void. Thomson et al. (2003) studied the effect of particle clustering on void damage rates in ductile failure of an aluminum alloy. They assumed a regular distribution of clustered particles and carried out a series of unit cell analyses. To predict fracture toughness, the void-containing cells need to be included in the crack tip region. Hom and McMeeking (1989) studied the interaction of a spherical void and the crack tip. Their results suggest that the void grows faster towards the crack tip direction than in the crack opening direction, revealing strong interaction between the growing void and the crack tip. They also demonstrated that the initially spherical void grows much slower than the initially cylindrical void. Kim et al. (2003) extended the 2D work of Tvergaard and Hutchinson (2002) by considering a row of spherical voids ahead of the crack front in the 3D SSY model.

Similar to the results obtained by Tvergaard and Hutchinson, Kim et al. found that transition from the void by void growth mechanism to the multiple voids interaction mechanism is controlled by the initial void volume fraction. Using results of a systematic unit cell analyses as the material failure criterion, they also presented a procedure to predict fracture initiation, subsequent crack growth and the J–R curve.

Most of the previous 3D analyses assume voids having spherical shape initially and consider only a single void or a single row of voids ahead of the crack tip. These analyses over-simplify the material microstructure and failure process. Many processed materials, such as rolled plates, have non-spherical voids and the void spacing is not uniform in all directions. Besides void volume fraction, void shape, void orientation and void distribution also have strong effect on the material failure mechanism and thus the fracture toughness. These issues are examined in this paper.

2. Void distribution and finite element modeling

This study considers the mode I, SSY problem, i.e., the plastic zone size is assumed to be small comparing to the geometric dimensions of the specimen. In ductile metals, voids often nucleate at relatively low stress levels due to fracture or decohesion of the large inclusions. For the purpose of analysis, voids are assumed to be present in the material at the onset of loading. Fig. 1(a) shows a periodical distribution of voids in the plane of crack propagation. In an attempt to rationalize fracture behavior, a local coordinate system is set up such that the x-axis represents the crack propagation direction, y-axis represents the crack opening direction and z-axis represents the thickness direction. Considering the existence of symmetry about the crack plane, only half of the region needs to be modeled. Except near free surfaces the deformation in the thickness direction can be assumed periodically symmetric. Neglecting the free surface effect allows us to apply the periodic boundary conditions and consider half of the void spacing distance in the thickness direction only, Fig. 1(b). Boundary conditions on the symmetry planes normal to z-direction are prescribed as

$$\begin{aligned} u_z &= 0, \\ t_x &= 0, \\ t_y &= 0, \end{aligned} \tag{1}$$

where u_z represents the displacement component in z-direction, t_x and t_y represent the components of surface traction in x and y directions respectively.

Three types of initial void shapes, spherical shape, prolate shape, and oblate shape, are considered. Fig. 2 shows the geometrical representation of the voids. The prolate and oblate voids are assumed to be

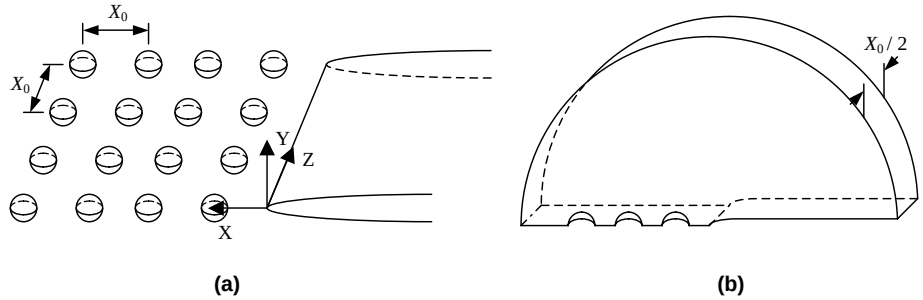

Fig. 1. (a) Periodical distribution of voids in the plane of crack propagation. (b) Domain of the boundary value problem.

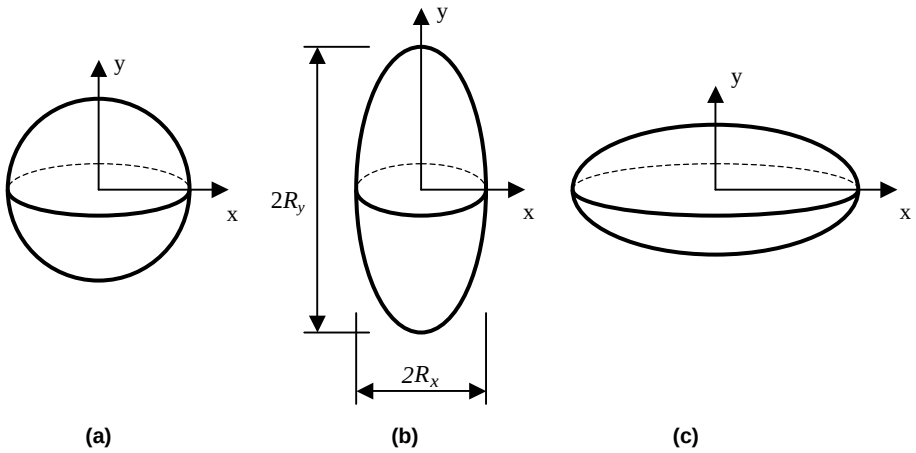

Fig. 2. Geometric representation of voids: (a) spherical void, (b) prolate void, and (c) oblate void.

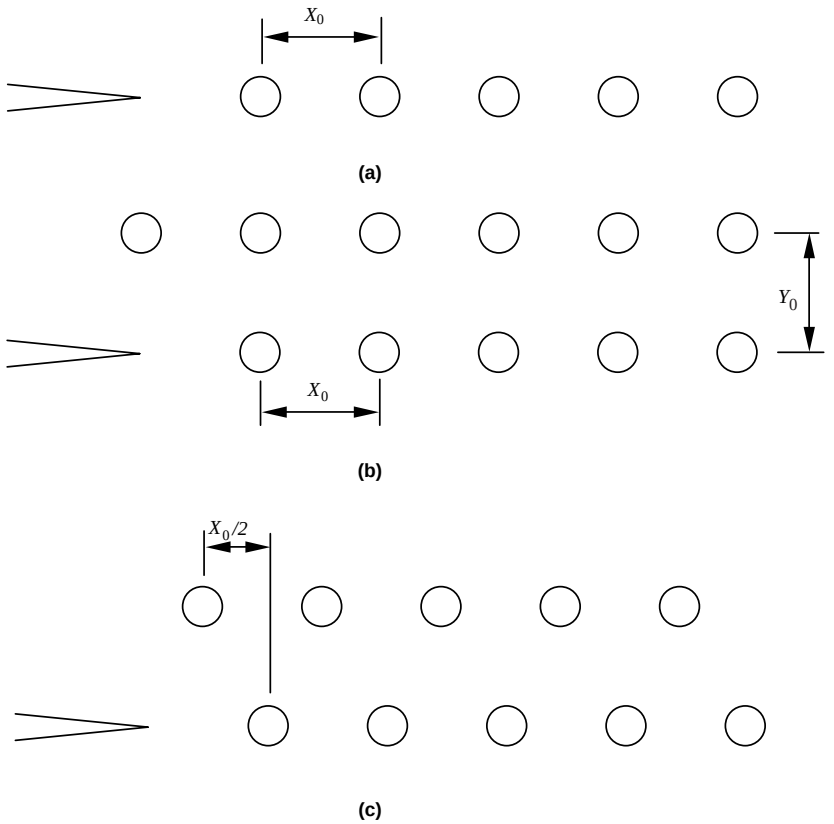

Fig. 3. Different initial void arrangements considered in this study.

axisymmetric about the y-axis and an initial aspect ratio is defined as $W_0 = R_{0y}/R_{0x}$. Therefore, $W_0 = 1$ corresponds to the spherical shape, $W_0 > 1$ corresponds to the prolate shape, and $W_0 < 1$ corresponds to the oblate shape.

Several initial void arrangements are considered in this study. In Fig. 3(a), only one row of voids are included in the model. The voids are directly ahead of the crack tip. The spacing between adjacent voids is X_0, which is the same as the distance from the first void to the crack tip. In Fig. 3(b), two rows of void are considered. The distance between the two rows is Y_0 and a parameter λ_0 is defined as the ratio of the void spacing in y-direction to the void spacing in x-direction, $\lambda_0 = Y_0/X_0$, measuring the relative void spacing. In Fig. 3(c), voids in the second row are shifted towards the $x = 0$ plane by a distance of $X_0/2$.

To resolve the crack tip deformation field and enhance convergence of the nonlinear iterations, the finite element mesh contains an initial root radius at the crack tip. Previous studies have shown that the influence of initial root radius becomes negligible if it is sufficiently small comparing to the void spacing. Here the initial root radius of the crack tip is taken to be $0.01X_0$. Numerical solutions are generated by imposing displacements of the elastic, asymptotic mode I field (plane strain) on the outer circular boundary. In this study, the radius of the outer circular boundary is taken to be $10{,}000X_0$ to assure the small scale yielding conditions being satisfied. The displacements at the outer boundary are given by

$$\begin{aligned} u_x &= \frac{1+v}{E}\sqrt{\frac{r_0}{2\pi}}\left\{K_{\mathrm{I}}\cos\frac{\theta}{2}\left(2-4v+2\sin^2\frac{\theta}{2}\right)\right\}, \\ u_y &= \frac{1+v}{E}\sqrt{\frac{r_0}{2\pi}}\left\{K_{\mathrm{I}}\sin\frac{\theta}{2}\left(4-4v-2\cos^2\frac{\theta}{2}\right)\right\}, \end{aligned} \tag{2}$$

where K_{I} represents the mode I stress intensity factor, (r, θ) denote the crack tip polar coordinates, and r_0 is the radius of the outer circular boundary of the SSY model. Loading of the SSY model proceeds by imposing displacement increments on the outer boundary according to the asymptotic fields.

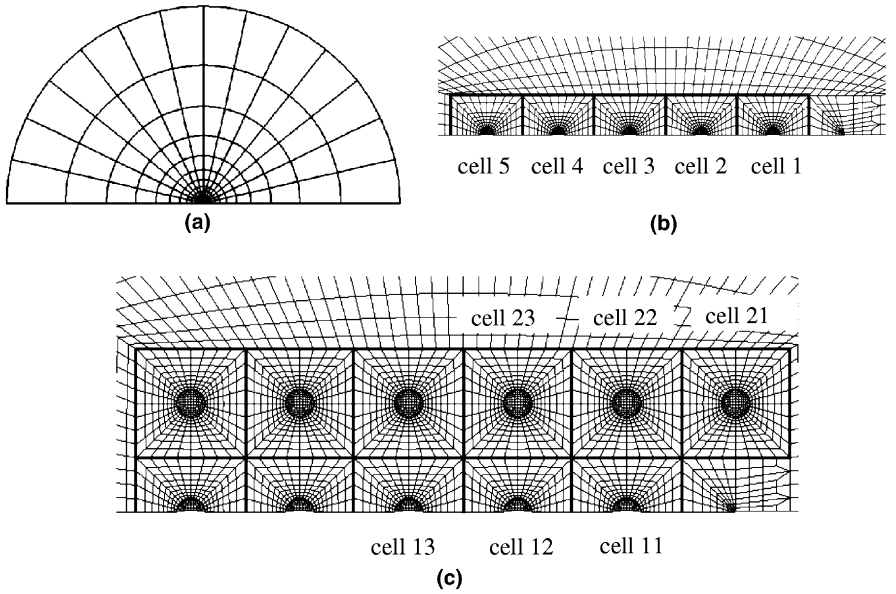

Fig. 4. (a) A typical finite element mesh of the SSY model. (b) Close-up of the crack tip region containing a row of five voids. (c) Close-up of the crack tip region containing two rows of voids.

Fig. 4(a) shows a typical finite element mesh of the SSY model. Close-up of the crack tip region is shown in Fig. 4(b) and (c) for finite element modeling containing one row and two rows of voids respectively. A typical mesh containing two rows of voids consists of 18,000 twenty-node, isoparametric, brick elements (86,000 nodes) with reduced integration.

It is natural to consider the material ahead of the crack tip as an array of unit cells with each unit cell containing a void at its center. The ratio of the void volume to the volume of the cell (including the void) defines the void volume fraction of the material. For models having a single row of voids as shown in Fig. 4(b), the cells are labeled with increasing numbers starting from the crack tip. For models having two rows of voids, e.g., Fig. 4(c), the cells are labeled using indices ij, where i refers to the row number and j refers to the position from the $x = 0$ plane, i.e., cell 21 refers to the first cell from the crack tip on the second row.

The material chosen for this study obeys the power-law hardening (true) stress–strain relation

$$\begin{aligned} \varepsilon &= \frac{\sigma}{E} \quad \sigma \leqslant \sigma_0, \\ \varepsilon &= \frac{\sigma_0}{E}\left(\frac{\sigma}{\sigma_0}\right)^{1/N} \quad \sigma > \sigma_0, \end{aligned} \tag{3}$$

where $E = 200$ GPa, $\sigma_0 = 600$ MPa, $v = 0.3$, and $N = 0.1$, which is representative of structural steel having an intermediate strength and moderate strain hardening. The stress–strain relation is implemented in ABAQUS (2001) by using the UHARD user subroutine.

3. Results and discussion

3.1. Void growth mechanisms

Previous studies (Tvergaard and Hutchinson, 2002; Kim et al., 2003) suggest that there exist two failure mechanisms, single void growth mechanism and multiple voids interaction mechanism. The single void growth mechanism is explained by the interaction of the crack tip with the nearest void and the subsequent advance of the crack tip from one void to the neighboring void. The multiple voids interaction mechanism is described by the simultaneous interaction of multiple voids positioned on a plane ahead of the crack tip both during initiation and stable crack growth. Here we examine the effects of the initial relative void spacing, void pattern, void shape and void volume fraction on the void growth and material failure mechanisms.

3.1.1. Model containing a single row of voids

We start with the model containing only one row of five voids ahead of the crack tip as illustrated in Fig. 3(a). Three void shapes, spherical ($W_0 = 1$), prolate ($W_0 = 4$) and oblate ($W_0 = 0.25$), with different values of initial void volume fraction, $f_0 = (4/3)\pi R_{0x}^2 R_{0y}/(X_0^2 Y_0)$, are considered in the analyses. Here the initial shape of the unit cells ahead of the crack tip is assumed to be cubic, i.e., $X_0 = Y_0$. In Fig. 5, the ratio of the void volume to its initial value, V/V_0, is plotted as a function of crack tip loading, $J/(X_0\sigma_0)$, for each of the five voids ahead of the crack tip. The trend remains the same for all six cases considered here, Fig. 5(a)–(f). For $f_0 = 0.001$, only the first void from the crack tip has significant volume increase as $J/(X_0\sigma_0)$ increases, which manifests the single void growth mechanism. As f_0 increases, the interaction among voids becomes important, which in turn elevates the void growth rate. As a result, the ductile failure mechanism transits from single void growth to multiple voids interaction. When $f_0 = 0.005$, several voids grow almost simultaneously as $J/(X_0\sigma_0)$ increases. These results agree with the general conclusion drawn by Tvergaard and Hutchinson (2002) and Kim et al. (2003).

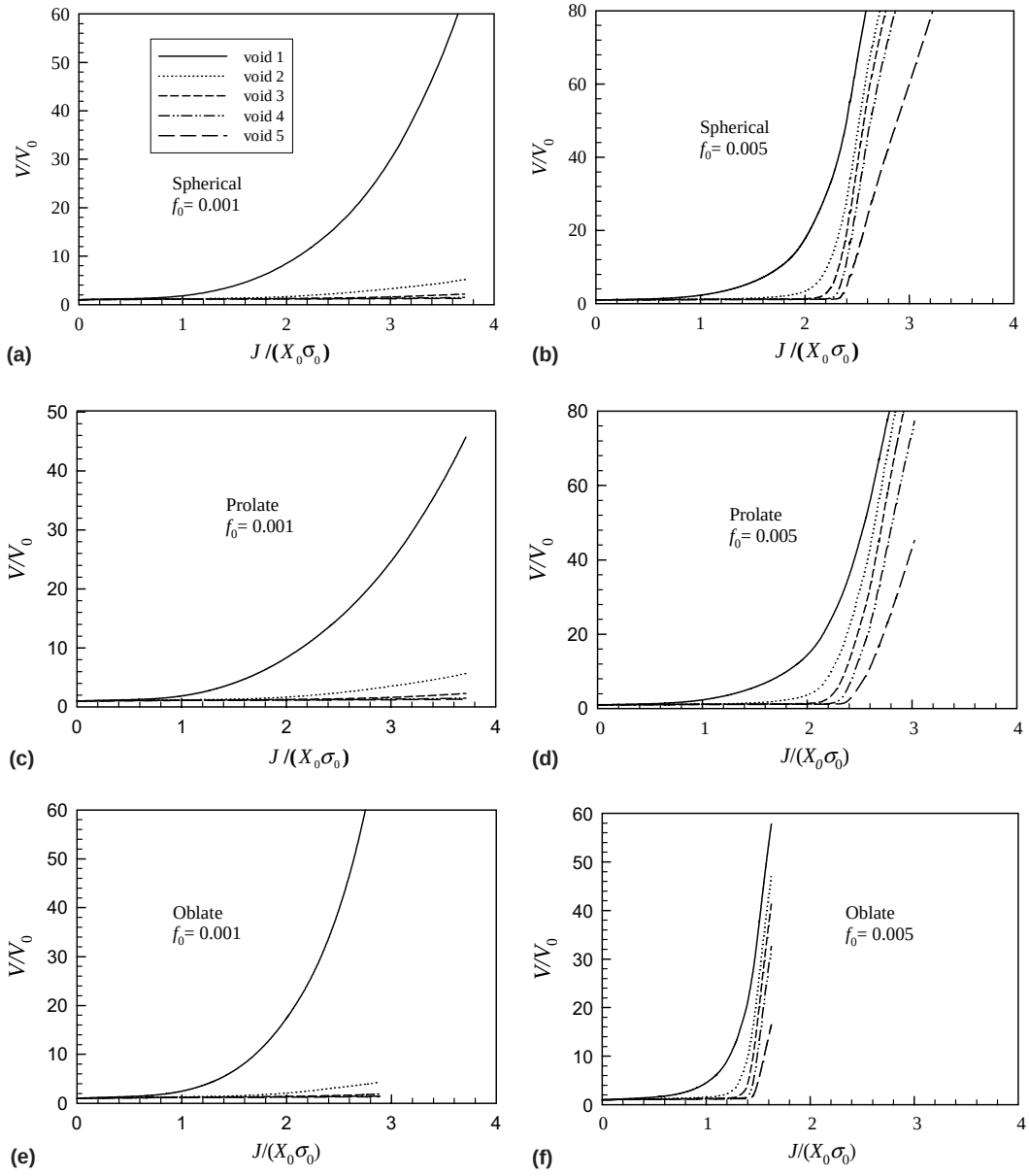

Fig. 5. Comparison of the void growth rates in cells ahead of the crack tip showing transition of the void growth mechanism from void by void growth to multiple voids interaction as initial void volume fraction increases. Here the finite element models contain only one row of voids.

Fig. 6 compares the growth rate of the first void as a function of $J/(X_0\sigma_0)$ for the six cases. It can be seen that both initial void shape and void volume fraction have strong effect on the rate of void growth. For the same initial void volume fraction, the oblate void grows faster than the spherical void and the spherical void grows faster than the prolate void, i.e., the void growth rate decreases with W. For the same initial void

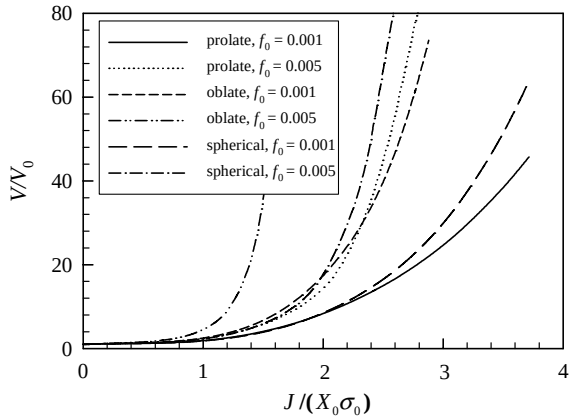

Fig. 6. Comparison of the growth rate of the first void for different cases showing the effects of the initial void shape and void volume fraction on the void growth rate.

shape (W_0), the void which has a larger initial volume fraction exhibits a faster growth rate, i.e., the void growth rate increases with f_0.

To demonstrate the significance of void interaction on material failure. The results obtained using the model containing a row of five voids are compared with the results of a model containing only one void ahead of the crack tip. As an example, we consider the spherical void shape. Fig. 7(a) compares the growth rate of the nearest void from crack tip between the single void model and the model containing five voids and Fig. 7(b) compares the reduction of the ligament between the crack tip and the nearest void between the two models. The comparison are made for two initial void volume fractions, $f_0 = 0.001$ and $f_0 = 0.01$. For the case of low initial porosity, the two models do not reveal any noticeable difference in void growth rate and the reduction rate of the ligament between the crack tip and the nearest void. However, there is a noticeable difference for the case of high initial porosity. Interaction among multiple voids elevates the void growth rate and accelerates the failure process. Therefore, the finite element model must include sufficient number of voids when the failure mechanism is due to multiple voids interaction. Earlier studies, e.g., Hom and McMeeking (1989), often consider a single void ahead of the crack tip. These studies under-predict void growth in high porosity materials and over-estimate the fracture toughness.

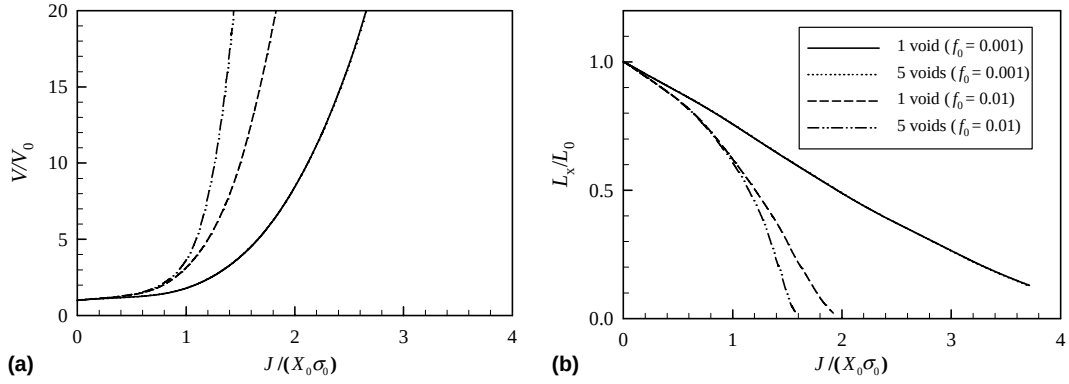

Fig. 7. Comparison of (a) the growth rate of the first void from the crack tip and (b) the size reduction ratio of the first ligament obtained using the single void model and the model containing five voids.

3.1.2. Model containing two rows of voids ($\lambda_0 = 1$)

Previous studies only consider a single row of voids positioned on the plane of crack propagation. But in real materials voids also exist off the plane of crack propagation. We first consider the void pattern shown in Fig. 3(b) with equal initial void spacing in x and y directions, i.e., $\lambda_0 = 1$. For the prolate and oblate voids, the initial aspect ratios are taken to be 4 and 0.25 respectively. Fig. 8 shows the ratio of the void volume to its initial value, V/V_0, as a function of crack tip loading, $J/(X_0\sigma_0)$, for several voids ahead of the crack tip. For $f_0 = 0.001$, only the first void directly ahead of the crack tip experiences significant growth

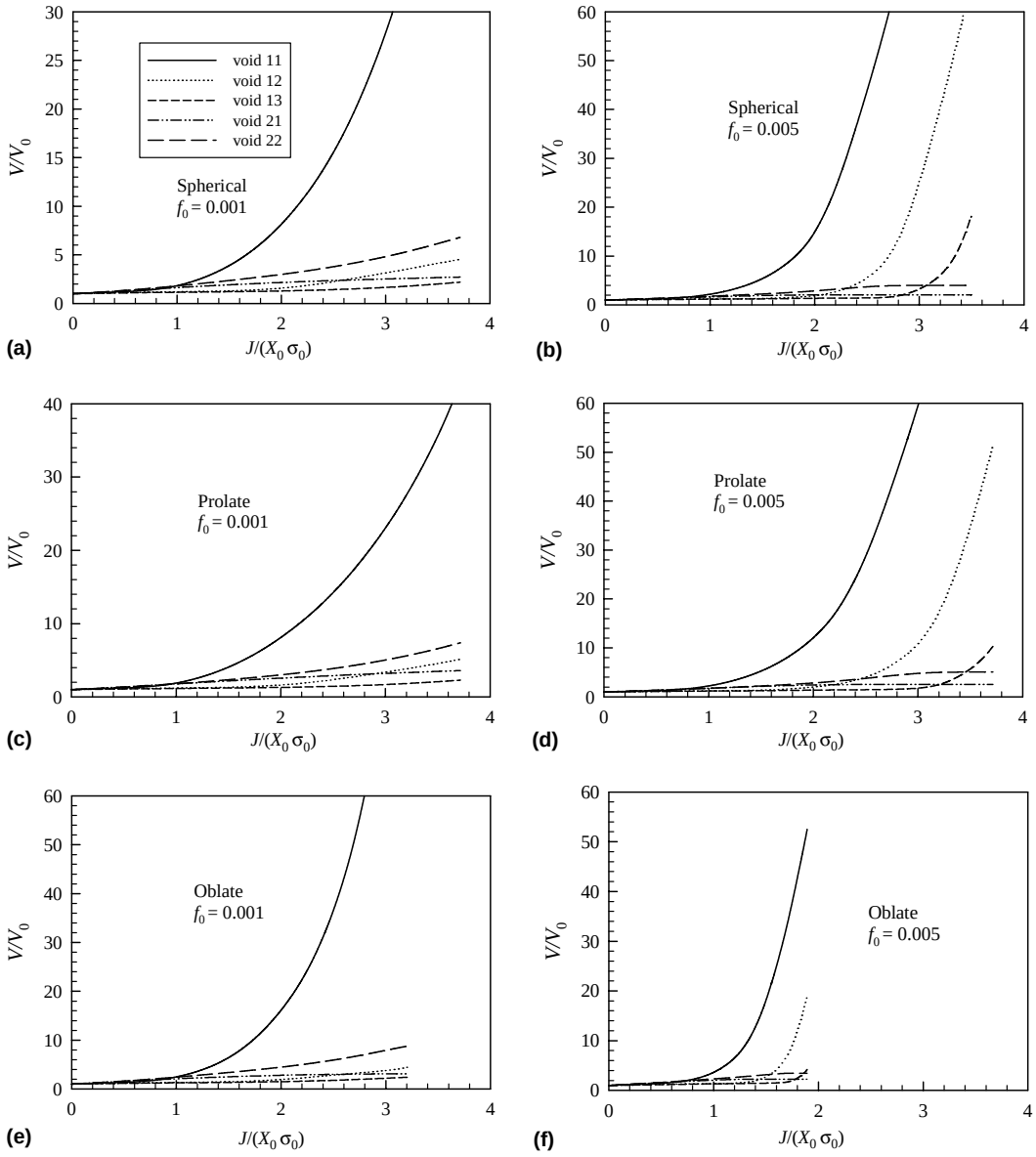

Fig. 8. Comparison of the void growth rates in several cells in the crack tip region. Here the finite element models contain two rows of voids with equal initial void spacing in x and y directions.

as J increases, which demonstrates the single void growth mechanism. The growth rates of the voids in the first row hardly show any difference from the results obtained using models containing only one row of voids. This suggests that void interaction between different rows is negligible. It is worth noting that the second void in the second row (void 22) has noticeable volume increase.

For $f_0 = 0.005$, the first two voids in the first row experience significant volume increase as J increases, Fig. 8(b), (d) and (f). This is different from the results shown in Fig. 5(b), (d) and (f), where all five voids grow almost simultaneously. Clearly, the presence of the voids in the second row decreases the growth rates of the voids in the first row. In contrast to the model containing only one row of voids where the material above the void-containing cells is dense, for the model containing two rows of voids, the material surrounding the first row cells is porous. The stress triaxiality in porous materials cannot reach as high as in dense materials. Therefore, the void growth rate is smaller in the model containing two rows of voids. The decrease in growth rate is more significant as the distance from the void to the crack tip increases. Consequently, one should expect that the predicted J–R curve to be steeper using models containing two rows of voids than using models containing only a single row of voids.

To demonstrate the transition to multiple voids interaction mechanism, we consider a model containing two rows of spherical voids with $f_0 = 0.01$. As expected, multiple voids grow concurrently as J increases, Fig. 9. Similar results can be obtained by considering prolate and oblate voids.

In summary, the presence of the second row voids has negligible effects on the growth of the voids on the plane directly ahead of the crack front when the initial void volume fraction is small and the void growth mechanism is void by void. Consequently, for computational simplicity, it is sufficient to include only one row of voids in the finite element model when the f_0-value is small. However, as f_0 increases, the effects of the second row voids become more and more significant. Their presence delays the transition of the fracture mechanism from void by void growth to multiple voids interaction. Therefore, for large f_0-values, the finite element should include multiple rows of voids.

3.1.3. Effect of relative void spacing

In above calculations, the void spacing is assumed to be equal in all three directions, i.e., the unit cells are cubic. This assumption is not valid for some materials, e.g., the rolled plate where the void spacing is shorter in the thickness direction. In this subsection the effect of relative void spacing is examined. The finite element models used in Section 3.1.2 containing two rows of voids are modified such that λ_0 takes different

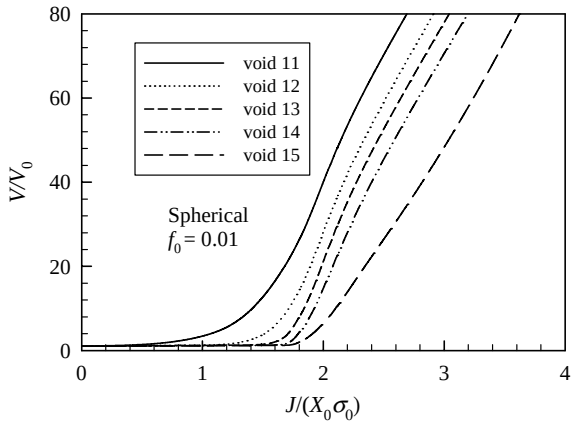

Fig. 9. Volume increase of voids on the plane of crack propagation computed using a model containing two rows of spherical voids showing the multiple voids interaction mechanism. Here $f_0 = 0.01$.

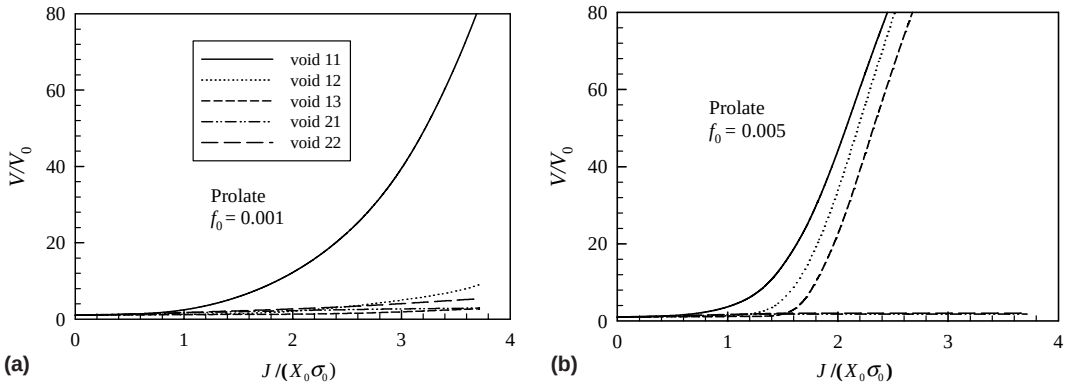

Fig. 10. Comparison of the void growth rates in cells in the crack tip region. Here the finite element models contain two rows of prolate voids with $\lambda_0 = 1.5$.

values. For the case of $\lambda_0 = 1.5$, the V/V_0 versus $J/(X_0\sigma_0)$ curves for several voids ahead of the crack tip are shown in Fig. 10, where the initial void shape is prolate with $W_0 = 4$. When $f_0 = 0.001$, the results displayed in Fig. 10(a) are similar to those shown in Fig. 8(c): only the void directly ahead of the crack tip exhibits significant growth. However, when $f_0 = 0.005$, the results are quite different: Fig. 10(b) displays a multiple voids interaction mechanism in contrast to the void by void growth mechanism shown in Fig. 8(d). Therefore, an increase in λ_0-value intensifies the interaction among neighboring voids and reduces the f_0 value at which transition from the void by void growth mechanism to the multiple voids interaction mechanism occurs.

For the case of $\lambda_0 = 2/3$, the V/V_0 versus $J/(X_0\sigma_0)$ curves are shown in Fig. 11 for the oblate voids with an initial aspect ratio of 0.25. Comparing with the results shown in Fig. 8(e) and (f), the smaller λ_0-value reduces the interaction among the first row voids and delays the occurrence of the multiple voids interaction mechanism.

3.1.4. Effect of void pattern

Here the void pattern shown in Fig. 3(c) is considered, where voids in the second row are shifted towards the $x = 0$ plane by a distance of $X_0/2$. The spherical void shape is used in the demonstration and the void

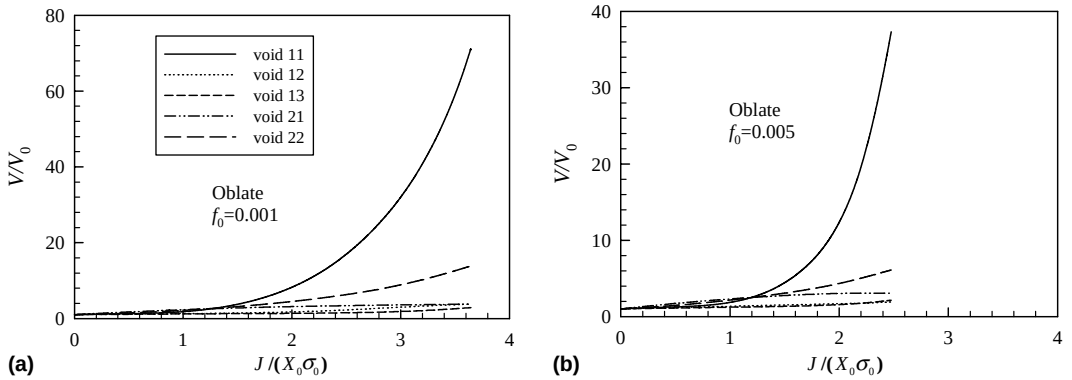

Fig. 11. Comparison of the void growth rates in cells in the crack tip region. Here the finite element models contain two rows of oblate voids with $\lambda_0 = 2/3$.

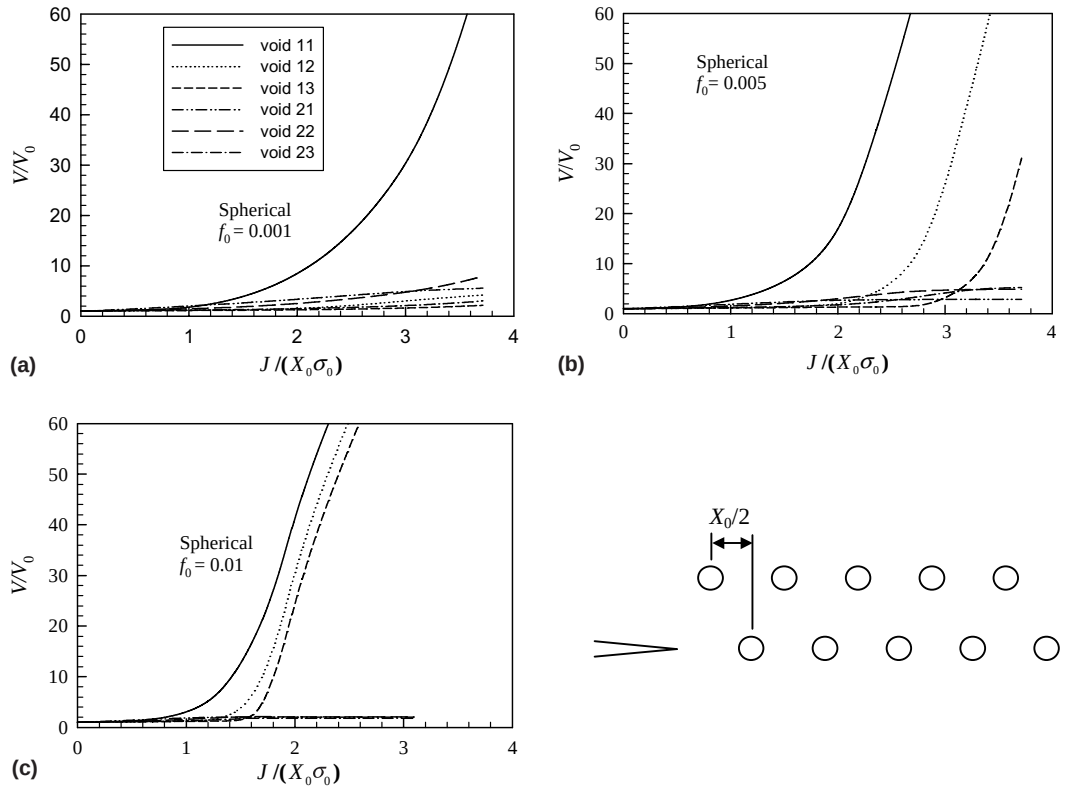

Fig. 12. Comparison of the void growth rates in several cells in the crack tip region. Here the finite element models contain two rows of spherical voids and the voids in the second row are shifted towards the $x = 0$ plane by a distance of $X_0/2$.

spacing is assumed to be equal in x and y directions, i.e., $\lambda_0 = 1$. Fig. 12 shows the V/V_0 versus $J/(X_0\sigma_0)$ curves for three initial f_0 values, 0.001, 0.005, and 0.01. For $f_0 = 0.001$, only the first void directly ahead of the crack tip experiences significant volume increase as J increases. For $f_0 = 0.005$, the second and third voids start to show significant volume increase at higher J levels. As f_0 increases to 0.01, multiple voids in the first row grow almost concurrently. These results are the same as those shown in Figs. 8(a), (b) and 9. Change of void pattern by shifting the positions of voids in the second row has negligible effect on the grow rates of voids in the first row.

3.2. Material failure criterion

Macroscopic crack initiation is said to have occurred upon coalescence of the growing voids with the crack tip. Several mechanistic observations have been put forth to explain void coalescence. Coalescence can occur through shear band formation, or through formation of "void sheets", or through impingement of neighboring voids. It is very difficult to implement these coalescence mechanisms directly to the numerical model. As a viable alternative, a critical ligament reduction ratio has been introduced to indicate the onset of void coalescence (Tvergaard and Hutchinson, 2002; Kim et al., 2003). However, as shown by Kim et al. (2003), the critical ligament ratio cannot be taken as a constant. The dependencies of the critical ligament reduction ratio on the macroscopic stress state of the representative material volume, the initial

void shape and void volume fraction, and other factors can be obtained by conducting a series of unit cell analysis.

3.2.1. Macroscopic behavior of a representative material volume in the crack tip region

As shown in Fig. 3, the material in the crack tip region can be considered as an array of cells. Each cell is a representative material volume containing a void at its center. The macroscopic stresses and strains of the cells in the SSY model are computed as follows:

$$\begin{aligned} \Sigma_{ij} &= \frac{1}{V}\int_V \sigma_{ij}\,\mathrm{d}V, \\ E_{ij} &= \sum_{\mathrm{inc}=1}^{n\mathrm{inc}} \Delta E_{ij}. \end{aligned} \tag{4}$$

In above equations, Σ_{ij} represent the macroscopic stress components, σ_{ij} represent the (true) stress components of the matrix, V is the volume of the cell including the void, E_{ij} represent the macroscopic (true) strain components, inc is the index for a load increment and $n$inc is the total number of increments for a given load. The macroscopic strain increments ΔE_{ij} are calculated from the displacement increments Δu_i as $\Delta E_{ij} = \frac{1}{2V}\int_S(\Delta u_i n_j + \Delta u_j n_i)\,\mathrm{d}S$. The cell volume V is computed as $V = \int_S x_1 n_1\,\mathrm{d}S$, where S is the outside surface of the cell with n_i being the components of the normal vector of S. These values are evaluated using the finite element integration scheme (Zienkiewicz, 1977). The macroscopic effective stress (Σ_e), hydrostatic stress (Σ_h), and effective strain (E_e) are given by

$$\begin{aligned} \Sigma_\mathrm{e} &= \frac{1}{\sqrt{2}}\left[(\Sigma_{xx}-\Sigma_{yy})^2 + (\Sigma_{yy}-\Sigma_{zz})^2 + (\Sigma_{zz}-\Sigma_{xx})^2\right]^{1/2}, \\ \Sigma_\mathrm{h} &= \frac{1}{3}(\Sigma_{xx}+\Sigma_{yy}+\Sigma_{zz}), \\ E_\mathrm{e} &= \frac{\sqrt{2}}{3}\left[(E_{xx}-E_{yy})^2 + (E_{yy}-E_{zz})^2 + (E_{zz}-E_{xx})^2\right]^{1/2}. \end{aligned} \tag{5}$$

Since the deformed shape of the cells in the SSY model is symmetric about the y and z planes, the macroscopic shear stress/strain components are all zero and are not included in Eq. (5).

To characterize the macroscopic stress state of the cell, the following stress ratios are introduced

$$T = \frac{\Sigma_\mathrm{h}}{\Sigma_\mathrm{e}}, \quad \rho_1 = \frac{\Sigma_{xx}}{\Sigma_{yy}}, \quad \rho_2 = \frac{\Sigma_{zz}}{\Sigma_{yy}}. \tag{6}$$

Zhang et al. (2001) and Kim et al. (2004) studied the effects of the triaxial stress state and found that the stress triaxiality ratio T alone cannot uniquely characterize the effect of macroscopic stress state on void growth and coalescence. The Lode parameter should be used to distinguish different stress states having the same stress triaxiality ratio. Defining

$$\tan\theta = \frac{2\Sigma_{zz}-\Sigma_{yy}-\Sigma_{xx}}{\sqrt{3}(\Sigma_{yy}-\Sigma_{xx})}, \tag{7}$$

Zhang et al. (2001) and Kim et al. (2004) showed that a cell when subject to the same stress triaxiality ratio would tend to react differently when θ is different. The stress triaxiality ratio along with the parameter θ can be used to specify stress state.

Fig. 13 shows the variation of Σ_e, T, ρ_1 and θ as the increase of applied load J for five cells ahead of the crack tip in the model containing a single row of voids as shown in Fig. 3(a). Here the initial void shape is prolate ($W_0 = 4$) and the initial void volume fraction is $f_0 = 0.005$. As expected, the stress triaxiality ratio T and the parameter θ are not constant during the loading history. The triaxiality ratio increases with applied

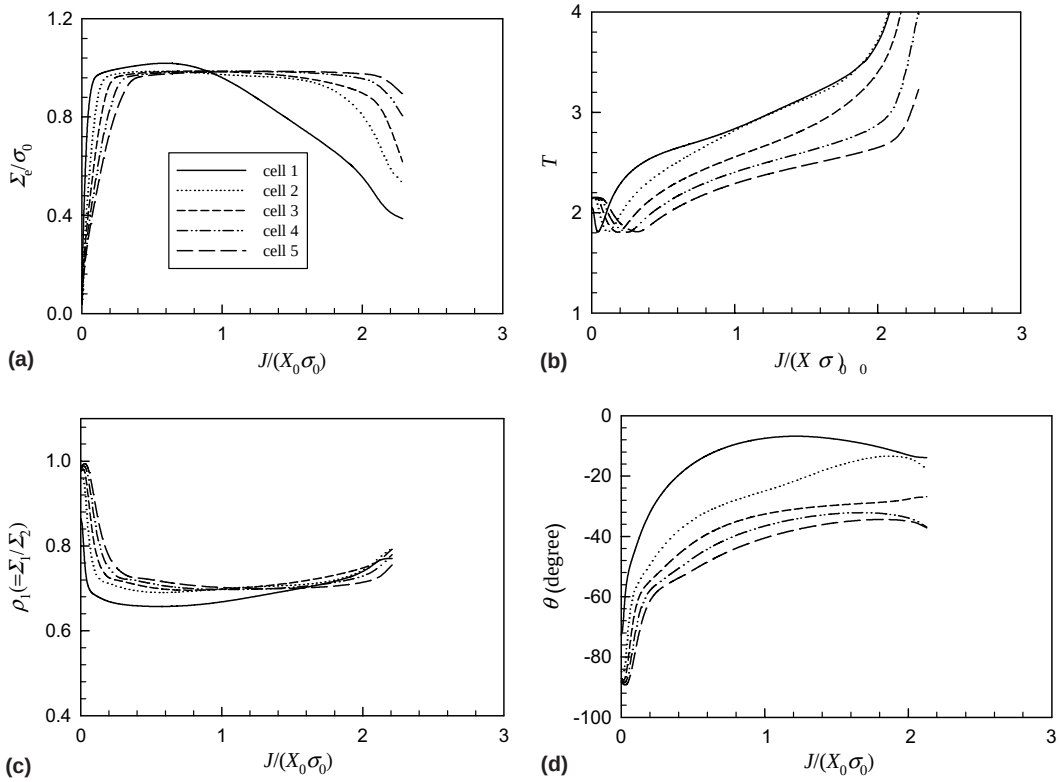

Fig. 13. Variation of the macroscopic (a) effective stress Σ_e, (b) stress triaxiality ratio T, (c) stress ratio ρ_1, and (d) Lode parameter θ with the applied load J for several cells ahead of the crack tip. Here the finite element model contains a single row of prolate voids with $f_0 = 0.005$.

J in the plastic deformation region of the cell. A sudden increase in triaxiality ratio occurs due essentially to collapse of the cell and rapid drop of Σ_e. The parameter θ also increases with the applied load. This is because the stress ratio in the thickness direction becomes larger as the applied J increases. Interestingly, the macroscopic stress ratio ρ_1 for each cell remains almost a constant after macroscopic plasticity occurs. Similar results are obtained when different void shapes and initial void volume fractions are considered.

Fig. 14 compares the variations of Σ_e, T, ρ_1 and θ of the first cell in models containing two rows of voids with different void arrangements. The prolate void shape ($W_0 = 4$) with initial void volume fractions of 0.001 and 0.005 is considered here. The trends are similar to those shown in Fig. 13 and it seems that the relative void spacing (λ_0) does not have a significant effect on the macroscopic stress state of the first cell.

3.2.2. Critical ligament reduction ratio

Considering the material composed of void-containing cells, failure of the ligament between neighboring voids corresponds to the process of internal necking. Coalescence (internal necking) will occur when the macroscopic deformation of the cell shifts to a uniaxial strain state (Koplik and Needleman, 1988). To utilize this idea, we consider the representative material volumes subjected to the loading conditions similar to the cells in the SSY models discussed in the previous section. A one-eighth symmetric finite element mesh of the unit cell containing an initially spherical void at its center is shown in Fig. 15(a), where Fig. 15(b)

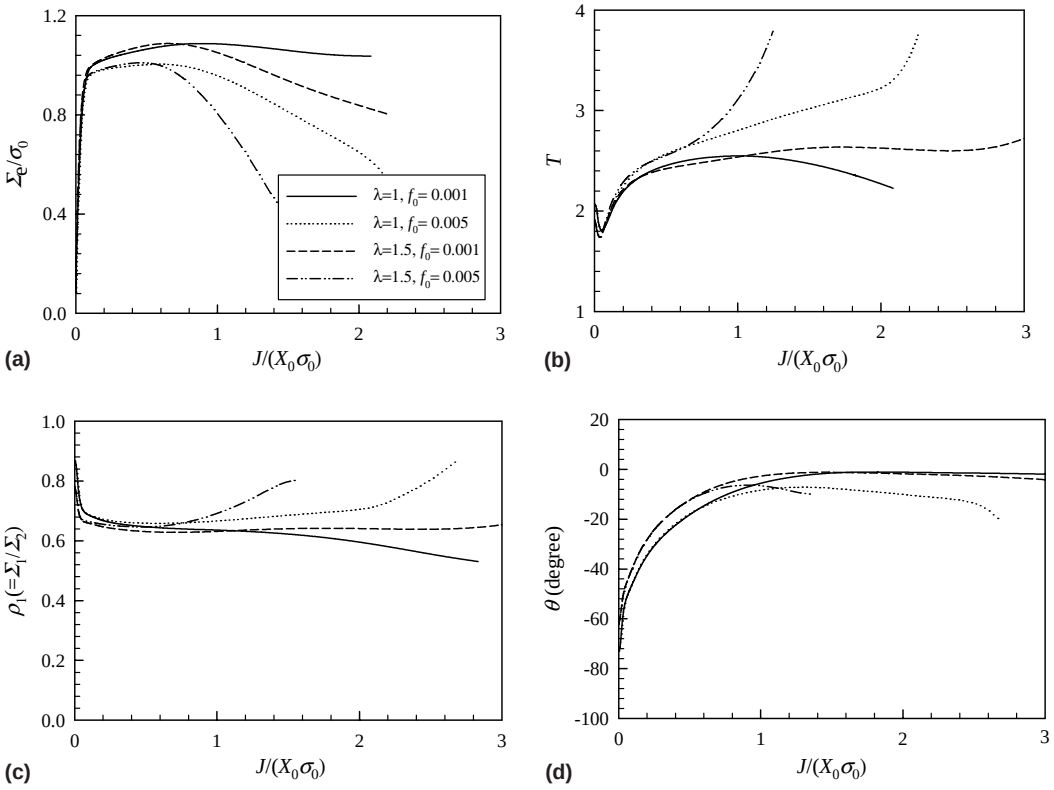

Fig. 14. Variations of Σ_e, T, ρ_1, and θ of the first cell in models containing two rows of prolate voids with different void arrangements and initial void volume fractions.

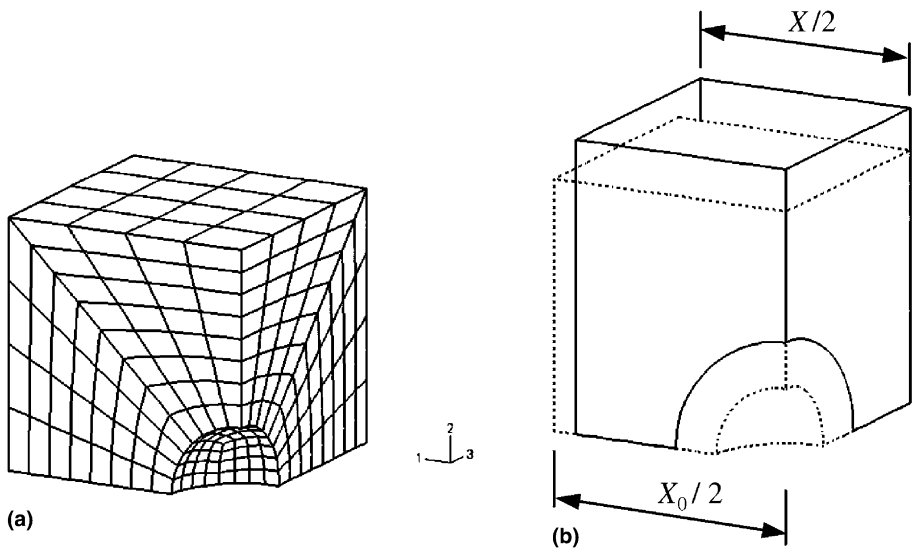

Fig. 15. (a) A one-eighth symmetric finite element mesh and (b) the deformed shape for the unit cell containing a centered, spherical void.

display the resultant deformed shape of the model. Displacement boundary conditions are prescribed on the outer surfaces of the cell. The displacement component in z-direction is constrained on the face normal to the z-axis. The displacement components are specified on the faces perpendicular to the x-axis and y-axis incrementally using the procedure developed by Faleskog et al. (1998) so that the macroscopic stress ratio $\rho_1 = \Sigma_{xx}/\Sigma_{yy}$ remain constant during the loading history. Details of how to prescribe the boundary conditions can be found in Kim et al. (2004).

Variation of the deformed cell width in x-direction with the macroscopic effective strain of the cell, shown in Fig. 16(a), reveals the shift to uniaxial straining. Here results for three initial void shapes ($W_0 = 0.25$, 1, 4) are presented. The cells are initially cubic ($\lambda_0 = 1$) and the initial void volume fraction is $f_0 = 0.005$. The macroscopic stress ratio ρ_1 is taken as 0.54. Fig. 16(b) shows the macroscopic effective stress versus effective strain for the cell displaying the macroscopic softening. The circles in Fig. 16 represent the onset of uniaxial straining mode, i.e., void coalescence.

At the onset of void coalescence, the ligament reduction ratio, defined as the ratio of the current ligament length (shortest distance between two adjacent voids in x-direction) to the initial ligament length, can be calculated. The critical ligament reduction ratio is denoted as χ_c. To determine χ_c, we conduct unit cell analyses for the cases of various initial relative void spacing, void shape, void volume fraction and different values of the macroscopic stress ratio ρ_1. It is found that χ_c depends on λ_0, W_0, f_0, and ρ_1. An increase in either initial void volume fraction, or void aspect ratio, or applied stress ratio tends to increase χ_c. Table 1 lists the χ_c-values for different cases.

3.3. Fracture initiation toughness

Using the critical ligament reduction ratios obtained in Section 3.2.2 and the SSY models described in Section 2, the fracture initiation toughness can be predicted. Here the fracture initiation is defined as when the first void coalesces with the crack tip. To determine the onset of fracture initiation, it is necessary to estimate the macroscopic stress ratio ρ_1 of the ligament between the crack tip and the first void. However, it is difficult to calculate the ligament stress ratio ρ_1 directly. We approximate the ligament ρ_1 value by extrapolation using the macroscopic stress ratios calculated for the first two cells. With the ρ_1 of the liga-

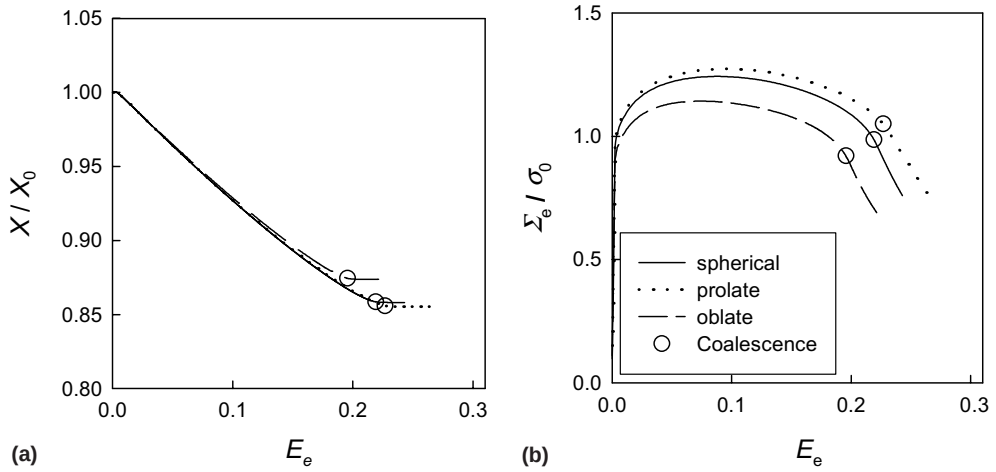

Fig. 16. (a) Variation of the deformed cell width in x-direction with the macroscopic effective strain of the cell revealing the shift to uniaxial straining. (b) Macroscopic effective stress versus effective strain of the cell displaying the macroscopic softening. Here $\rho_1 = 0.54$, $f_0 = 0.005$ and the symbols denote the onset of coalescence.

Table 1
χ_c values for different cases

Void shape	Spherical		Prolate				Oblate			
λ_0	1		1		1.5		1		2/3	
	f_0									
ρ_1	0.001	0.005	0.001	0.005	0.001	0.005	0.001	0.005	0.001	0.005
0.44	0.2373	0.3382	0.2538	0.3294	0.3280	0.4265	0.2102	0.3301	0.2310	0.2493
0.54	0.3514	0.4289	0.3711	0.4491	0.4631	0.5601	0.3093	0.4066	0.2574	0.2779
0.64	0.4563	0.5076	0.4884	0.5563	0.6091	0.7075	0.4010	0.4693	0.3108	0.2840
0.74	0.5562	0.5947	0.6125	0.6920	0.7697	0.8519	0.5096	0.5169	0.3457	0.3029

ment estimated, the χ_c-values in Table 1 can be used to determine the applied J at which the first void coalesces with the crack tip. This applied J value can be regarded as the fracture initiation toughness (J_{Ic}). Simple linear interpolation is used when the ρ_1-value of the ligament is different from the ρ_1-values listed in Table 1.

Using the above approach, the variation of J_{Ic} with the initial relative void spacing, void pattern, void shape and void volume fraction can be predicted. Fig. 17(a) shows the predicted dependence of J_{Ic} on the

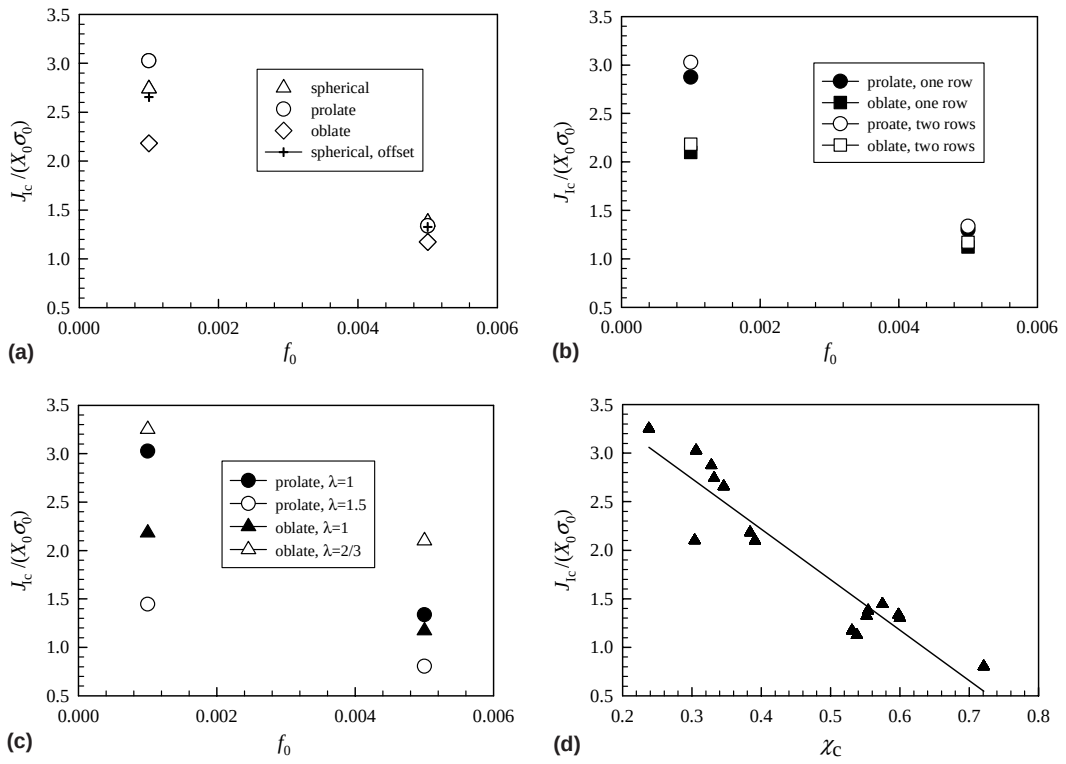

Fig. 17. (a) Predicted dependence of the fracture initiation toughness on the initial void volume fraction using models containing two rows of voids with different initial shapes. (b) Comparison of the predicted J_{Ic}-values using models containing two rows of voids with those using models containing one row of voids. (c) Effect of the initial relative void spacing on fracture initiation toughness. (d) Relationship between J_{Ic} and the χ_c-value for the first ligament.

initial void volume fraction using the finite element models containing two rows of spherical, prolate ($W_0 = 4$), and oblate ($W_0 = 0.25$) voids. In general, the value of J_{Ic} increases as f_0 decreases. For the same value of f_0, J_{Ic} is highest when the initial void shape is prolate and lowest when the initial void shape is oblate, i.e., J_{Ic} increases with W_0. The difference in predicted J_{Ic} for different void shapes becomes less significant as f_0 becomes large. Change of the void pattern by shifting the positions of the voids in the second row (indicated by the cross symbol) does not result in noticeable difference in J_{Ic}.

Fig. 17(b) compares the predicted J_{Ic}-values using models containing two rows of voids with those using models containing one row of voids. No noticeable difference is observed between the predicted J_{Ic}-values using the two models. This rationalizes the approaches used in the previous studies, e.g., Gu (2000), Tvergaard and Hutchinson (2002), and Kim et al. (2003), where only one row of voids are included in the finite element model. However, it is very important to point out that the single row void model over-predicts the growth rates of voids other than the first one when f_0 is large (see the results in Section 3.1) resulting in a flatter J–R curve. To correctly predict the J–R curve for a material having large initial volume fraction, the finite element model should include multiple rows of voids.

Fig. 17(c) demonstrates the effect of relative void spacing on the fracture initiation toughness. The results show that the fracture toughness decreases with λ_0. This is easy to understand because larger λ_0-value means shorter relative void spacing in the x-direction and thus earlier coalescence of the voids with crack tip.

As defined previously, J_{Ic} is determined as the applied J-value when the reduction of the ligament length between the first void and the crack tip reaches the critical ratio χ_c. The χ_c for the first ligament varies with the initial relative void spacing, void pattern, void shape and void volume fraction. If we collect the χ_c-values for all the cases presented in Fig. 17(a)–(c) and plot χ_c versus the corresponding J_{Ic}-value for each case, we can reveal a trend of J_{Ic} decreasing with the increase of χ_c, Fig. 17(d). It is interesting to note that the relationship between J_{Ic} and the χ_c-value for the first ligament can be approximated by a straight line.

It is worth noting that in this study coalescence is defined as the onset of internal necking. Most engineering materials contain more than one populations of inclusions and/or second phase particles. Due to localized plastic deformation between the enlarged voids and between the void and the crack tip, small particles in the ligaments will nucleate secondary microvoids. Rapid growth and coalescence of secondary voids will accelerate the ligament failure process. Nucleation and growth of secondary microvoids are not taken into account in this study, and therefore, the critical ligament reduction ratios determined above can be regarded as the lower bound values and the fracture toughness values predicted using those critical ligament reduction ratios are the upper bound values for the material.

3.4. Analysis of the anisotropy in fracture initial toughness of a C–Mn steel

The method described in previous sections can be used to analyze the anisotropy of a rolled steel plate. Bauvineau (1996) and Bauvineau et al. (1996) conducted an investigation of the ductile fracture of a rolled C–Mn steel, measuring the fracture initiation toughness (J_{Ic}) of the material for the 'SL' and 'TL' directions: $J_{Ic}(SL) \sim 50$ kJ/m^2 and $J_{Ic}(TL) \sim 100$ kJ/m^2. Here, L is the longitudinal direction, T is the transverse direction and S is the short transverse direction. SL means that the crack is in a plane orthogonal to the S direction and propagates in the L direction, while TL means that the crack is in a plane orthogonal to the T direction, propagating in the L direction. They also performed detailed metallographic analyses of the inclusion population, mainly MnS particles. The volume fraction of MnS inclusions was determined as 0.0025. This value can be considered as the initial void volume fraction, f_0, because void nucleation at inclusions occurs at relatively low stress levels. The inclusions are flat and elongated, presenting a preferential orientation due to the rolling process and display an ellipsoidal shape with mean diameters of 28, 15 and 3 μm in the L, T and S directions respectively and distance between inclusions as 179, 83, 64 μm in the TL, LS and TS planes respectively. Based on these data, we adopt $W_0 = 1.7$, $X_0 = 83$ μm and $\lambda_0 = 1$

Table 2
Microstructural parameters and fracture initiation toughness of a C–Mn steel

Direction	f_0	W_0	X_0 (μm)	λ_0	J_{Ic} (exp.) (kJ/m^2)	J_{Ic} (pred.) (kJ/m^2)
TL	0.0025	1.7	83	1	100	123
SL	0.0025	0.13	179	1	50	71

for the TL specimen and $W_0 = 0.13$, $X_0 = 179$ μm and $\lambda_0 = 1$ for the SL specimen. The value of $\lambda_0 = 1$ is taken for simplicity. The tensile properties of the material at the test temperature can be characterized by $\sigma_0 = 190$ MPa and $n = 0.27$. Pardoen and Hutchinson (2003) analyzed these experiments using a continuum damage model, the Gologanu–Leblond–Devaux model. Their numerical predictions are in reasonable agreement with the experimental results.

Here we use the discrete void model presented in previous sections to analyze the anisotropy of fracture initiation toughness of the C–Mn steel in TL and SL directions. Since we are only interested in predicting J_{Ic}, the computational models used in these analyses contain only one row of five voids directly ahead of the initial crack. Table 2 summarizes the parameters characterizing the material and the comparison between the measured and predicted fracture initiation toughness (J_{Ic}). The difference in toughness between the two directions of propagation is well captured, and the predicted and measured fracture toughness values are in reasonable agreement given the uncertainty in identifying the void spacing.

4. Concluding remarks

In this study, effects of the initial relative void spacing, void pattern, void shape and void volume fraction on ductile fracture toughness are analyzed using three-dimensional, small scale yielding models, where voids are assumed to pre-exist in the material and are explicitly modeled using refine finite elements. Based on our detailed analyses, the following remarks can be made.

(1) Our analyses re-affirm the two distinct void growth mechanisms put forth by Tvergaard and Hutchinson (2002), i.e., void by void growth mechanism for materials containing small initial void volume fractions and multiple voids interaction mechanism for materials containing large initial void volume fractions. Our results reveal that, besides the initial void volume fraction, other factors also affect void growth mechanism when the initial void volume fraction is large. Voids deviated from the crack growth plane reduce the interaction among voids on the crack growth plane and delay the transition from void by void growth mechanism to multiple voids interaction mechanism. Increase of λ_0 (relative void spacing) intensifies the interaction among neighboring voids and facilitates the transition from void by void growth mechanism to multiple voids interaction mechanism. Change of the void distribution pattern by shifting the positions of second row voids does not affect the growth rates of voids in the plane of crack propagation. Our results also show that when other parameters are the same, the oblate void grows faster than the spherical void and the spherical void grows faster than the prolate void.

(2) A critical ligament reduction ratio (χ_c), determined from unit cell analysis, is introduced to denote material failure and it is found that χ_c varies with the initial relative void spacing, void pattern, void shape and void volume fraction. The fracture initiation toughness (J_{Ic}) is determined as the applied J-value when the reduction of the ligament length between the first void and the crack tip reaches the critical ratio χ_c. Our results reveal that J_{Ic} increases with decreasing f_0. For the same value of f_0, J_{Ic} is highest when the initial void shape is prolate and lowest when the initial void shape is oblate. Existence of the second row voids and change of void pattern do not result in noticeable difference in J_{Ic}. However, the initial relative void spacing has significant effect on J_{Ic}. These results can be used to explain why various degrees of fracture toughness anisotropy are observed in industrial alloys.

(3) Previous studies often use finite element models containing a single row of voids. Our analyses suggest that these simplified models are sufficient when the initial void volume fraction remains small. When the initial void volume fraction is large, these simplified models can predict J_{Ic} with sufficient accuracy but cannot predict the correct J–R curve. In order to predict the J–R curve for a material having large initial volume fraction, the finite element model should include multiple rows of voids.

Acknowledgments

This research was made possible through research funding provided by the Office of Naval Research (N00014-02-1-0423) and by the Ohio Board of Regents.

References

ABAQUS/Standard User's Manual, Version 6.2, 2001. Hibbit, Karlsson and Sorensen Inc.

Aravas, N., McMeeking, R.M., 1985a. Finite element analysis of void growth near a blunting crack tip. J. Mech. Phys. Solids 33, 25–49.

Aravas, N., McMeeking, R.M., 1985b. Microvoid growth and failure in the ligament between a hole and blunt crack tip. Finite element analysis of void growth near a blunting crack tip. Int. J. Fract. 29, 21–38.

Arun Roy, Y., Narasimhan, R., 1999. A finite element investigation of the effect of crack tip constraint on hole growth under mode I and mixed mode loading. Int. J. Solids Struct. 36, 1427–1447.

Bauvineau, L., 1996. Approche locale de la rupture ductile: application a un acier carbone–manganese. Ph.D. thesis, Ecole National Superieure des Mines de Paris, France.

Bauvineau, L., Burlet, H., Eripret, C., Pineau, A., 1996. Modelling ductile stable crack growth in a C–Mn steel with local approaches. J. Phys. IV 6 (C6), 33–42.

Brocks, W., Klingbeil, D.A., Kumecke, G., Sun, D.Z., 1995. Application of the Gurson model to ductile tearing resistance. In: Kirk, M., Bakker, A. (Eds.), Constraint Effects in Fracture Theory and Applications, ASTM STP 1244. ASTM, Philadelphia, PA, pp. 232–254.

Brown, L.M., Embury, J.D., 1973. In: Proceedings of the 3rd International Conference on Strength of Metals and Alloys. Institute of Metals, London, p. 164.

Faleskog, J., Gao, X., Shih, C.F., 1998. Cell model for nonlinear fracture analysis—I. Micromechanics calibration. Int. J. Fract. 89, 355–373.

Gao, X., Faleskog, J., Shih, C.F., 1998a. Cell model for nonlinear fracture analysis—II. Fracture-process calibration and verification. Int. J. Fract. 89, 375–398.

Gao, X., Faleskog, J., Shih, C.F., Dodds, R.H., 1998b. Ductile tearing in part-through cracks: experiments and cell-model predictions. Eng. Fract. Mech. 59, 761–777.

Gu, I., 2000. Finite element analyses of the deformation around holes near crack tip and their implications to the J-resistance curve. Fatig. Fract. Eng. Mater. Struct. 23, 943–952.

Gurson, A.L., 1977. Continuum of ductile rupture by void nucleation and growth: Part I—Yield criteria and flow rules for porous ductile media. J. Eng. Mater. Tech. 99, 2–55.

Hom, C.L., McMeeking, R.M., 1989. Void growth in elastic–plastic materials. J. Appl. Mech. 56, 309–317.

Kim, J., Gao, X., Srivatsan, T.S., 2003. Modeling of crack growth in ductile solids: a three-dimensional analysis. Int. J. Solids Struct. 40, 7357–7374.

Kim, J., Gao, X., Srivatsan, T.S., 2004. Modeling of void growth in ductile solids: effects of stress triaxiality and initial porosity. Eng. Fract. Mech. 71, 379–400.

Koplik, J., Needleman, A., 1988. Void growth and coalescence in porous plastic solids. Int. J. Solids Struct. 24, 835–853.

Kuna, M., Sun, D.Z., 1996. Three-dimensional cell model analyses of void growth in ductile materials. Int. J. Fract. 81, 235–258.

Le Roy, G., Embury, J.D., Edward, G., Ashby, M.F., 1981. A model of ductile fracture based on the nucleation and growth of voids. Acta Metall. 29, 1509–1522.

Pardoen, T., Hutchinson, J.W., 2003. Micromechanics-based model for trends in toughness of ductile metals. Acta Mater. 51, 133–148.

Rice, J.R., Johnson, M.A., 1969. The role of large crack tip geometry changes in plane strain fracture. In: Kannine, M.F., Adler, W.F., Rosenfield, A.R., Jaffee, R.I. (Eds.), Inelastic Behavior of Solids. McGraw-Hill, New York, p. 641.

Thomson, C.I.A., Worswick, M.J., Pilkey, A.K., Lloyd, D.J., 2003. Void coalescence within periodic clusters of particles. J. Mech. Phys. Solids 51, 127–146.

Tvergaard, V., 1982. On localization in ductile materials containing spherical voids. Int. J. Fract. 18, 237–252.

Tvergaard, V., Hutchinson, J.W., 2002. Two mechanisms of ductile fracture: void by void growth verse multiple void interaction. Int. J. Solids Struct. 39, 3581–3597.

Xia, L., Shih, C.F., Hutchinson, J.W., 1995. Computational approach to ductile crack growth under large scale yielding conditions. J. Mech. Phys. Solids 43, 389–413.

Yan, C., Mai, U.W., 1998. Effect of constraint on void growth near a blunt crack tip. Int. J. Fract. 92, 287–304.

Zhang, K.S., Bai, J.B., Francois, D., 2001. Numerical analysis of the influence of the Lode parameter on the void growth. Int. J. Solids Struct. 38, 5847–5856.

Zienkiewicz, O.C., 1977. The Finite Element Method, 3rd ed. McGraw-Hill, London.